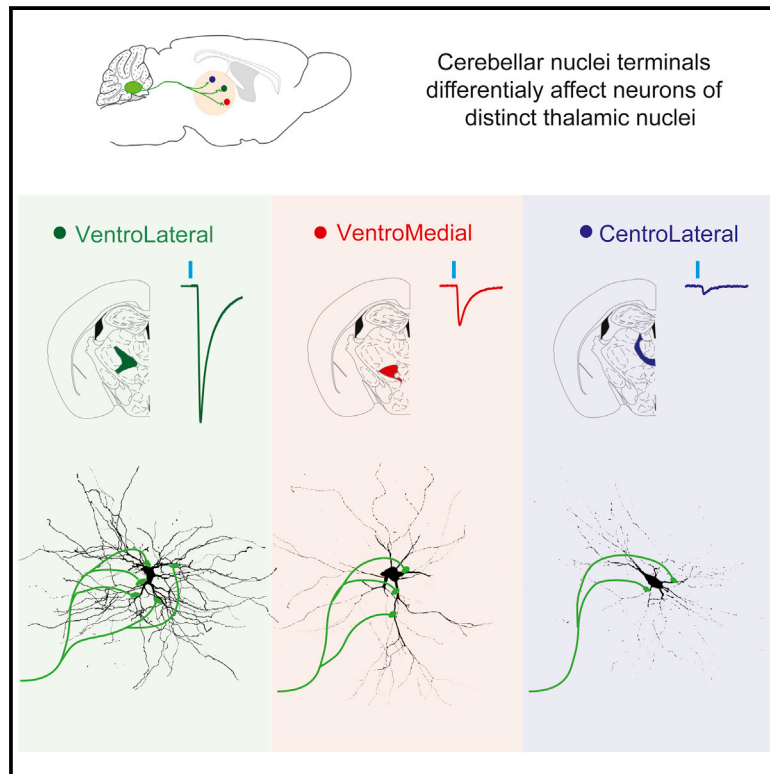


Differentiating Cerebellar Impact on Thalamic Nuclei

Graphical Abstract



Authors

Simona V. Gornati, Carmen B. Schäfer, Oscar H.J. Eelkman Rooda, Alex L. Nigg, Chris I. De Zeeuw, Freek E. Hoebeek

Correspondence

f.e.hoebeek@umcutrecht.nl

In Brief

In this study, Gornati et al. demonstrate that the impact of cerebellar nuclei axons on thalamic neurons varies per thalamic region. These findings provide insights into how the versatile cerebellum can have a differential effect on the many brain regions that it connects to.

Highlights

- Cerebello-thalamic axons form terminals of varying size in distinct thalamic nuclei
- Cerebello-thalamic responses vary in amplitude in distinct thalamic nuclei
- Repetitive stimuli depress cerebello-thalamic responses in all thalamic nuclei



Differentiating Cerebellar Impact on Thalamic Nuclei

Simona V. Gornati,^{1,6} Carmen B. Schäfer,^{1,6} Oscar H.J. Eelkman Rooda,^{1,2} Alex L. Nigg,³ Chris I. De Zeeuw,^{1,4} and Freek E. Hoebeek^{1,5,7,*}

¹Department of Neuroscience, Erasmus Medical Center, 3015 AA Rotterdam, The Netherlands

²Department of Neurosurgery, Erasmus Medical Center, 3015 AA Rotterdam, The Netherlands

³Department of Pathology, Optical Imaging Center, Erasmus MC, 3015 AA Rotterdam, The Netherlands

⁴Netherlands Institute for Neuroscience, Royal Academy for Arts and Sciences, 1105 BA Amsterdam, The Netherlands

⁵NIDOD Institute, Wilhelmina Children's Hospital and Brain Center Rudolf Magnus, University Medical Center Utrecht, 3508 AB Utrecht, The Netherlands

⁶These authors contributed equally

⁷Lead Contact

*Correspondence: f.e.hoebeek@umcutrecht.nl

<https://doi.org/10.1016/j.celrep.2018.04.098>

SUMMARY

The cerebellum plays a role in coordination of movements and non-motor functions. Cerebellar nuclei (CN) axons connect to various parts of the thalamo-cortical network, but detailed information on the characteristics of cerebello-thalamic connections is lacking. Here, we assessed the cerebellar input to the ventrolateral (VL), ventromedial (VM), and centrolateral (CL) thalamus. Confocal and electron microscopy showed an increased density and size of CN axon terminals in VL compared to VM or CL. Electrophysiological recordings *in vitro* revealed that optogenetic CN stimulation resulted in enhanced charge transfer and action potential firing in VL neurons compared to VM or CL neurons, despite that the paired-pulse ratio was not significantly different. Together, these findings indicate that the impact of CN input onto neurons of different thalamic nuclei varies substantially, which highlights the possibility that cerebellar output differentially controls various parts of the thalamo-cortical network.

INTRODUCTION

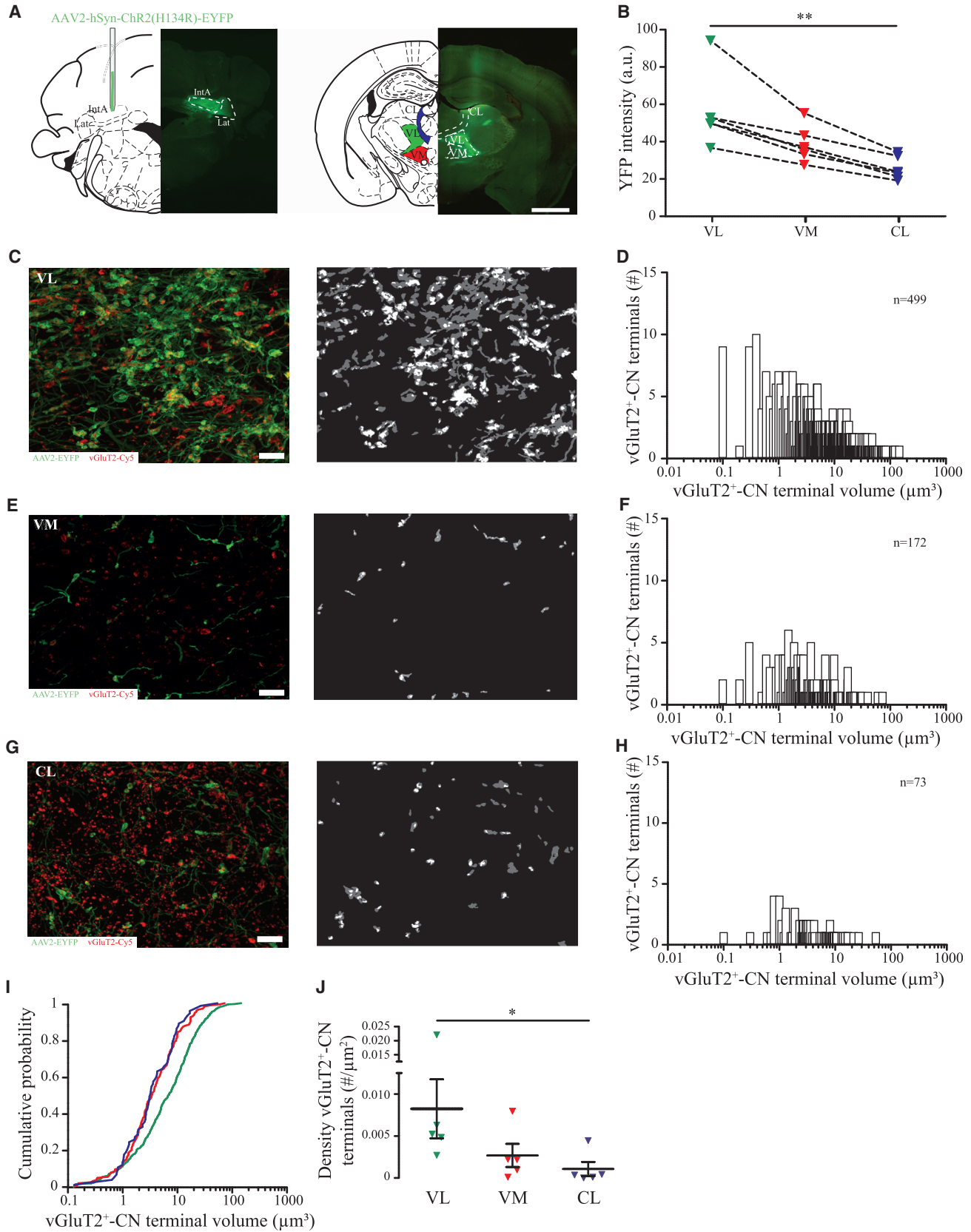
Cerebellar best-known functions are involved in coordinating motor activities. It contributes, for example, to learning new motor skills and prediction of the sensory consequences of action (Brooks et al., 2015; De Zeeuw and Ten Brinke, 2015; Manto et al., 2012). However, anatomical, physiological, and neuroimaging studies provide compelling evidence of the cerebellar involvement in various non-motor functions, like cognitive processes, language, and emotion, which became established in both animal models and patients (Bodranghien et al., 2016; Peter et al., 2016; Stoodley et al., 2017; Tsai et al., 2012; Wang et al., 2014). For instance, it was recently shown that manipu-

lating the cerebellar output affects sensorimotor integration by somatosensory and motor cortices and thereby could direct voluntary movements (Popa et al., 2013; Proville et al., 2014). The anatomical connections that underlie such wide impact of cerebellar activity on thalamo-cortical information processing do not only include cerebellar axons that innervate the premotor centers in the brainstem, like the red nucleus, but also a variety of nuclei within the thalamic complex, each of which has reciprocal connections with the cerebral cortex (Angaut et al., 1985; Aumann et al., 1994; Bentivoglio and Kuypers, 1982; Cohen et al., 1958; Daniel et al., 1987; Haroian et al., 1981; Herkenham, 1979; Teune et al., 2000).

The glutamatergic projection neurons located in the cerebellar nuclei (CN) connect to primary thalamic relay nuclei, like the ventrolateral (VL) nucleus, thalamic motor-associated nuclei such as the ventromedial (VM) nucleus, and additionally to intralaminar (IL) nuclei such as centromedian, parafascicular, and centrolateral (CL) nuclei (Aumann and Horne, 1996b; Teune et al., 2000). Historically, the thalamic relay neurons have been divided in two fundamentally different sets: parvalbumin-positive “core” neurons, which form topographically organized projections to middle layers of cerebral cortical patches, and calbindin-positive “matrix” neurons, which send more diffuse projections to the cortices and layers (Jones, 1998; Jones and Hendry, 1989). Provided that CN axons project to thalamic nuclei with high densities of core neurons, like VL, and with high densities of matrix neurons, like VM and CL, this connectivity of cerebellar-recipient thalamic nuclei suggests that the cerebellar impact differentially affects cortical information processing. Moreover, single-axon reconstructions of cerebellar-recipient zones within VL, VM, and CL reveal that their axons also spread throughout other regions (Deschênes et al., 1996b; Kuramoto et al., 2009, 2015), further highlighting that the cerebellar input can affect a wide range of thalamo-cortical networks and functions.

Apart from their connectivity to the cortex, the heterogeneity of cerebellar recipient thalamic nuclei also extends into the dendritic morphology. For instance, the cerebellar-recipient zones of the VL and VM have been shown to contain neurons with





(legend on next page)

“bushy” dendrites (Clascá et al., 2012; Kuramoto et al., 2009, 2015; Monconduit and Villanueva, 2005; Yamamoto et al., 1985) and thereby have a different appearance than CL neurons that show polarized dendritic branching (Deschênes et al., 1996b). This variability in the morphological aspects of thalamic neurons in the cerebellar-recipient nuclei corroborates the differential axonal projection patterns and suggests that the impact of cerebellar output on thalamic neurons varies for each target nucleus. However, the anatomical and electrophysiological data on the cerebello-thalamic projections lack an in-depth comparison of the cerebellar impact on the various thalamic targets.

So far, the electrophysiological studies that investigated the cerebello-thalamic projections focused on the VL nucleus. Intracellular recordings in this nucleus in anesthetized rats and cats revealed that electrical microstimulation of the CN neurons or the brachium conjunctivum triggered action potential firing (Bava et al., 1986; Rispal-Adel and Grangetto, 1977; Sawyer et al., 1994b; Uno et al., 1970), which matches the cerebellar-evoked responses in motor cortex (Rispal-Adel and Latreille, 1974; Steriade, 1995; Yoshida et al., 1966). Likewise, also single-pulse optogenetic stimulation in CN in the mouse brain has been proven to effectively control thalamo-cortical network activity (Kros et al., 2015; Proville et al., 2014). Morphological and ultrastructural analysis of the CN axon terminals in VL revealed that they typically synapse perisomatically on large-diameter dendrites and form large terminals with various mitochondria and release sites (Aumann and Horne, 1996a, 1996b; Aumann et al., 1994; Sawyer et al., 1994a). These findings function as a frame of reference, but a thorough understanding of the cerebellar impact on thalamo-cortical information processing is hampered by the lack of detailed *in vitro* cell physiological analysis and morphological characterization of the CN axonal projections throughout the various thalamic nuclei.

In order to elucidate how the cerebellar impact on thalamic neurons correlates to the specific nuclei, we studied the post-synaptic responses of thalamic relay neurons to selective stimulation of CN axons using *in vitro* whole-cell recordings. We focused on neurons in the VL, VM, and CL and correlated the electrophysiological data to the morphological details of the target neurons. Our results show that both presynaptic and postsynaptic aspects of the cerebello-thalamic transmission vary between these thalamic nuclei and thereby provide evidence for the functional diversification of the cerebellar impact on thalamo-cortical networks.

RESULTS

Thalamic Nuclei Receive Various Densities of CN Axons and Terminals

To assess the innervation of VL, VM, and CL thalamic nuclei by cerebellar axons in the mouse brain, we transfected CN neurons located mostly in, but not limited to, the interposed CN with a virally encoded ChR2-YFP-expressing construct (Figure 1A). In several mice, we found that the medial and lateral CN also contained ChR2-YFP-expressing neurons. In the thalamus, we found the level of intensity of this membrane-bound fluorophore to be highest in the VL (55.9 ± 8.0 a.u.) compared to VM (38.7 ± 3.9 a.u.) and CL (25.8 ± 2.3 a.u.) ($p = 0.529$ for VL versus VM, $p = 0.002$ for VL versus CL, $p = 0.136$ for VM versus CL, Kruskal-Wallis [K-W] tests, Dunn's correction; Figure 1B; Table S1).

To dissociate between the active CN terminals and passing axons, we chose to stain for vesicular glutamate transporter 2 (vGluT2), which has previously been shown to label CN axon terminals (Kuramoto et al., 2009; Rovó et al., 2012), and solely quantify the double-labeled vGluT2-positive (vGluT2⁺) ChR2-EYFP-expressing CN terminals. When we assessed these vGluT2⁺-CN terminals using stacks of high-magnification images acquired with confocal microscopy and subsequently applied custom-written image analysis scripts, we found that the VL nucleus was most densely populated by vGluT2⁺-CN terminals (total count, 499 vGluT2⁺-CN terminals; $N = 5$ mice; Figures 1C and 1D) with a mean volume of $12.45 \pm 0.74 \mu\text{m}^3$. As previously reported (Aumann et al., 1994), VM encompasses CN axons passing through, some of which send branches in the most medial part of the nucleus (Figure 1E). The number of vGluT2⁺-CN terminals in VM was lower compared to VL, and their volume was significantly smaller ($6.65 \pm 0.71 \mu\text{m}^3$; $n = 172$ terminals, $p < 0.001$, Kolmogorov-Smirnov [K-S] test; Figures 1F and 1I; Table S1). The CL nucleus showed the lowest number of vGluT2⁺-CN terminals, and their volume was statistically different from VL but not from VM ($5.85 \pm 0.90 \mu\text{m}^3$; $n = 73$ terminals; $p = 0.002$ for VL versus CL and $p = 0.966$ for VM versus CL, K-S test; Figures 1G–1I; Table S1). We observed a significantly higher density of vGluT2⁺-CN terminals in VL compared to CL ($p = 0.024$; K-W test), whereas the differences in density between VL-VM and VM-CL were not significantly different ($p = 0.334$ and $p = 0.865$, respectively; K-W tests; Figure 1J; Table S1). These data demonstrate that the cerebellar projection innervates preferentially VL and that these terminals are also bigger compared to VM and CL.

Figure 1. Variable Innervation of VL, VM, and CL Nuclei by CN Axons

(A) Schematic representation of the experiment. AAV injection in the interposed nucleus (left) and fluorescent (ChR2-EYFP) CN axons (right) throughout the thalamic complex (3 weeks postinjection) of the same mouse. The nuclei of interest are highlighted in green (VL), red (VM), and blue (CL). This color code will be applied throughout all the figures. Scale bar, 1 mm.

(B) YFP intensity signal in the three nuclei of interest ($N = 6$ mice).

(C, E, and G) Left: maximum intensity projection of Z-stack (14- μm thick) showing in green ChR2-EYFP-stained CN axons, and in red, vGluT2 staining for VL (C), VM (E) and CL (G). Right: the result of the colocalization mask; gray indicates ChR2-EYFP-stained axons, and white, vGluT2⁺ and EYFP.

(D, F, and H) Histograms showing vGluT2⁺-CN terminal volume and number for VL (D), VM (F), and CL (H) ($N = 5$ mice).

(I) Cumulative plot of the terminal volume (green, VL; red, VM; blue, CL) (VL versus CL, $p < 0.001$; VL versus VM, $p < 0.001$; and VM versus CL, $p = 0.966$; $N = 5$ mice, K-S test).

(J) Average density of vGluT2⁺-CN terminals (VL versus CL, $p = 0.024$).

Data are presented as mean \pm SEM. * $p < 0.05$, ** $p < 0.01$, *** $p < 0.001$. K-W test was used. For full statistical report, see Table S1.

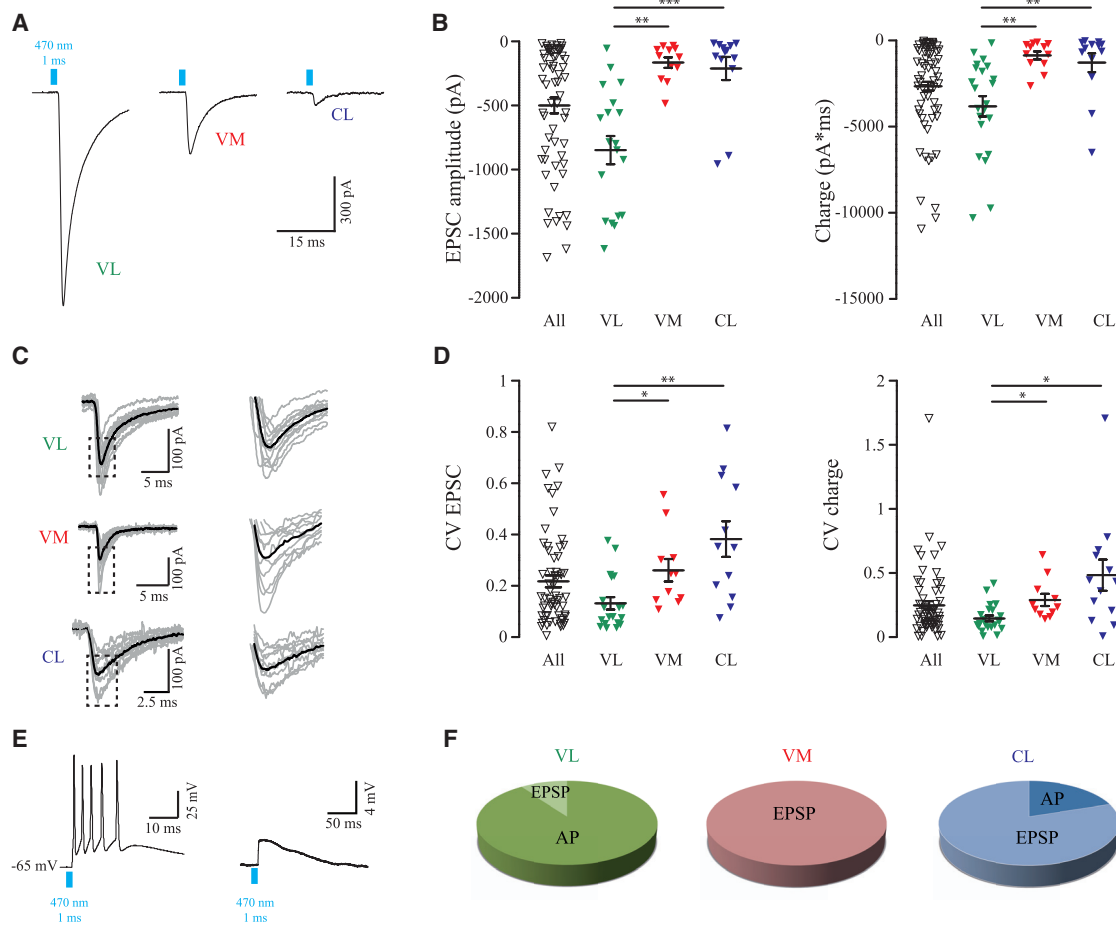


Figure 2. Charge Transfer between CN Axons and Thalamic Neurons Differs for VL, VM, and CL

(A) Optical wide-field stimulation of CN terminals (470 nm, 1-ms pulse length) evoked EPSCs of variable amplitude in VL, VM, and CL. (B) Quantification of EPSCs amplitude and charge for all recorded cells (n = 63 for EPSC amplitude and n = 65 for charge) and for the nuclei of interest (EPSC: VL, n = 19; VM, n = 12; CL, n = 13; charge: VL, n = 22; VM, n = 12; CL, n = 13, respectively; "All" category represents all cells recorded, of which some were not recovered by histology and therefore were not classified to a specific nucleus—note that all cells in VL, VM, and CL are also represented in All). (C) Example traces of EPSCs amplitude in gray and average trace in black. Note the variability in EPSC amplitude of individual responses. (D) Coefficient of variation (CV) for (left) EPSCs amplitude and (right) EPSC charge. (E) Example traces of (left) action potential (AP) firing or (right) excitatory postsynaptic potential (EPSP) evoked by single-pulse CN stimulation. (F) Pie charts representing responses to CN stimulation recorded in current-clamp mode (VL: n = 9 AP, n = 1 EPSP; VM: n = 3 EPSP; CL: n = 1 AP, n = 4 EPSP). Data are presented as mean \pm SEM. *p < 0.05, **p < 0.01. K-W was used. For full statistical report, see Table S2.

Basic Transmission Properties of Cerebello-Thalamic Synapses Differ across Thalamic Nuclei

It has been shown by sharp electrode recordings in anesthetized cats and rats that electrical stimulation of CN axons could elicit monosynaptic excitatory postsynaptic potentials (EPSPs) from which a fast spike could arise in VL relay cells (Sawyer et al., 1994b; Uno et al., 1970). To our knowledge, no data have been published about the postsynaptic currents underlying these changes in VL potentials, or about the postsynaptic responses of thalamic VM or CL cells. To gather these data, we performed whole-cell patch-clamp recordings of VL, VM, and CL neurons in acutely prepared thalamic slices of mice that received bilateral CN injections with ChR2-EYFP-encoding AAV-vectors, which transfected neurons located mostly, but not exclusively, in the interposed nuclei (Experimental Procedures). We selected the

recorded neurons based on their position in the slice, i.e., surrounded by ChR2-EYFP encoding CN axons, their monosynaptic responses to 470-nm optical stimulation (see below) and their anatomical location. Overall, we found that the resting membrane potential of VL (-71.6 ± 0.9 mV; n = 20), VM (-72.2 ± 2.0 mV; n = 11), and CL (-70.0 ± 1.4 mV; n = 14) neurons was not significantly different (p = 0.736, one-way ANOVA), but that the input resistance of CL neurons was significantly higher than in VL neurons (p = 1 for VL [n = 23] versus VM [n = 12]), p = 0.012 for VL versus CL (n = 14), and p = 0.175 for VM versus CL; K-W test). In all three thalamic nuclei, single light pulses (1 ms, 470 nm, applied through the objective) elicited an excitatory postsynaptic current (EPSC) (Figure 2A). These events were reliably blocked by bath application of the voltage-gated Na⁺-channel blocker tetrodotoxin (TTX) (n = 5 cells; >99%

decrease in charge transfer), which indicates that the postsynaptic events were triggered by action potential-driven release of glutamate from CN terminals (data not shown). The mean EPSC amplitude that we could maximally evoke was significantly higher in VL than in VM and CL (VL, -847.7 ± 109.5 pA; VM, -165.0 ± 40.2 pA; CL, -210.8 ± 89.2 pA; $p = 0.001$ for VL versus VM, $p < 0.001$ for VL versus CL, and $p = 1$ for VM versus CL; K-W tests), which was also represented in the evoked charge (VL, -3820 ± 595 pA*ms; VM, -862 ± 235 pA*ms; CL, -1284 ± 542 pA*ms; $p = 0.002$ for VL versus VM; $p = 0.001$ for VL versus CL, $p = 1$ for VM versus CL; K-W tests; Figure 2B; Table S2). The variability in optically stimulated EPSC amplitude and charge was quantified by calculating the coefficient of variation (CV) (Figure 2C). We found significant differences in the CV of EPSC amplitudes (VL, 0.13 ± 0.02 ; VM, 0.25 ± 0.04 , CL, 0.38 ± 0.07 ; $p = 0.031$ for VL versus VM, $p = 0.001$ for VL versus CL, $p = 1$ for VM versus CL, K-W tests, Dunn's correction; Figure 2D; Table S2) and of EPSC charge (VL, 0.13 ± 0.02 ; VM, 0.28 ± 0.04 ; CL, 0.47 ± 0.12 ; $p = 0.03$ for VL versus CL, $p = 0.025$ for VL versus VM, $p = 1$ for VM versus CL, K-W tests, Dunn's correction; Table S2). We found no significant correlation of the incubation time to the EPSC amplitude, nor to the CV of the EPSC amplitude ($p = 0.470$, $r_s = 0.116$ for EPSCs, and $p = 0.269$, $r_s = 0.161$ for CV, Spearman correlation), which supports the notion that the difference in postsynaptic responses is actually due to a difference in the charge transfer between CN axons in VL, VM, and CL neurons.

To establish the impact of neurotransmitter release from CN terminals on thalamic neurons' membrane potential, we also recorded a subset of cells in current clamp (Figure 2E). When stimulated at maximum light intensity, most VL neurons fired action potentials (9 cells out of 10), whereas most VM (3 out of 3) and CL neurons (4 out of 5; Figure 2F) did not. The probability to elicit an action potential was not related to the resting membrane potential of the cell ($p = 0.628$; $r_s = -0.127$, Spearman correlation). As we expected from the EPSC amplitudes, neurons in VL fired action potentials more readily than those in VM and CL.

Thalamic Responses Show Paired-Pulse Depression and Are Predominantly Sensitive to Iontropic Glutamate Receptor Blockers

Thalamic afferents are often categorized as "driver" or "modulator" (Sherman, 2014; Sherman and Guillery, 1998). This classification is partially determined by the response to repetitive stimulation of presynaptic terminals: driver synapses are thought to show paired-pulse depression (PPD), whereas modulator synapses evoke paired-pulse facilitation (PPF) (Groh et al., 2008; Reichova and Sherman, 2004; Seol and Kuner, 2015). Although cerebellar input to motor thalamus has been listed as driver input (Sherman, 2014), short-term synaptic dynamics of thalamic responses following repetitive CN stimulation in VL, VM, and CL still need to be evaluated. Here, we performed voltage-clamp recordings while stimulating the CN terminals repetitively with trains of light pulses at 10, 20, and 50 Hz (Figures 3A–3C). To evaluate the time course of the depression, we normalized EPSC amplitudes to the first peak amplitude (Figures 3D–3F).

In general, we found that the ratio between the amplitudes of the first two EPSCs showed a PPD at all frequencies tested (Figure 3G). At 50 Hz, the second EPSC showed a ~ 2 -fold reduction in amplitude compared to the initial one (VL, 0.52 ± 0.06 ; VM, 0.72 ± 0.12 ; CL, 0.41 ± 0.08), whereas lower-frequency stimulations showed a smaller effect on the PPD. At 20 Hz, the depression was around 30% of the first EPSC in all the nuclei (VL, 0.70 ± 0.02 ; VM, 0.77 ± 0.10 ; CL, 0.73 ± 0.07), whereas at 10 Hz only VL (0.80 ± 0.03) and VM (0.88 ± 0.04) neurons showed on average PPD but CL did not (1.08 ± 0.25) (Figure 3H). When we compared the PPD across all nuclei for each frequency, we found that the ratio between the first two responses did not show any significant difference between the nuclei (10 Hz, $p = 0.344$; 20 Hz, $p = 0.168$; 50 Hz, $p = 0.137$; K-W tests; Dunn's correction; Figure 3H; Table S3).

Next, we analyzed the subsequent responses to the train stimulation to determine the average sustained release of presynaptic terminals during high-frequency steady-state synaptic transmission (Figures 3A–3C). For this analysis, the average phasic EPSC amplitude within the train was normalized to the average first EPSC amplitude for each frequency and each nucleus. Across all recorded cells, we find normalized steady-state amplitudes of $64.4 \pm 3.1\%$ (VL), $71.3 \pm 6.9\%$ (VM), and $81.4 \pm 8.9\%$ (CL) at 10 Hz; $53.1 \pm 3.6\%$ (VL), $70.1 \pm 11.1\%$ (VM), and $85.2 \pm 28.0\%$ (CL) at 20 Hz; and $44.4 \pm 5.0\%$ (VL), $41.9 \pm 6.5\%$ (VM), and $39.1 \pm 7.7\%$ (CL) at 50 Hz (Figure 3I; Table S3). We found no significant differences between the values recorded per nucleus but did find that, in VL, the steady-state depression was significantly higher at 50 Hz than at 10 Hz ($p = 0.005$, K-W test; Figure 3I; Table S3). These data indicate that the general tendency for transmission at cerebello-thalamic synapses in VL, VM, and CL is to show a depression of neurotransmitter release in response to repetitive stimulation.

Our results indicate that the synaptic transmission at cerebello-thalamic synapses in VL, VM, and CL are glutamatergic, which matches previous *in vivo* findings on the excitatory responses of VL neurons evoked by microstimulation of the brachium conjunctivum or the neurons in CN (Bava et al., 1986; Rispal-Padel and Grangetto, 1977; Sawyer et al., 1994b; Uno et al., 1970). To elucidate whether these excitatory postsynaptic responses were mediated by ionotropic and/or metabotropic receptors, we next tested the effects of their selective blockage on the responses to 50-Hz stimulus trains. Upon wash-in of α -amino-3-hydroxy-5-methyl-4-isoxazole propionic acid receptor (AMPA) antagonist 2,3-dihydroxy-6-nitro-7-sulfamoyl-benzo[*f*]quinoxaline-2,3-dione (NBQX), the EPSC charge decreased from -74.6 ± 2.4 nA*ms to -28.0 ± 8.3 nA*ms, and following the wash-in of *N*-methyl-D-aspartate receptor (NMDAR) antagonist (2*R*)-amino-5-phosphonovaleric acid (APV), the EPSC charge decreased even further to -13.5 ± 4.3 nA*ms ($p < 0.001$, Friedman test; Figures 4A and 4B; Table S4). Further application of blockers for the metabotropic glutamate receptors (mGluRs) most abundantly expressed in thalamic neurons (3,4-dihydro-2H-pyranolo[2,3-*B*]quinolin-7-*YL*)-(cis-4-methoxycyclohexyl)-methanone [JNJ] for mGluR1 and 2-methyl-6-(phenylethynyl)pyridine [MPEP] for mGluR5; Liu

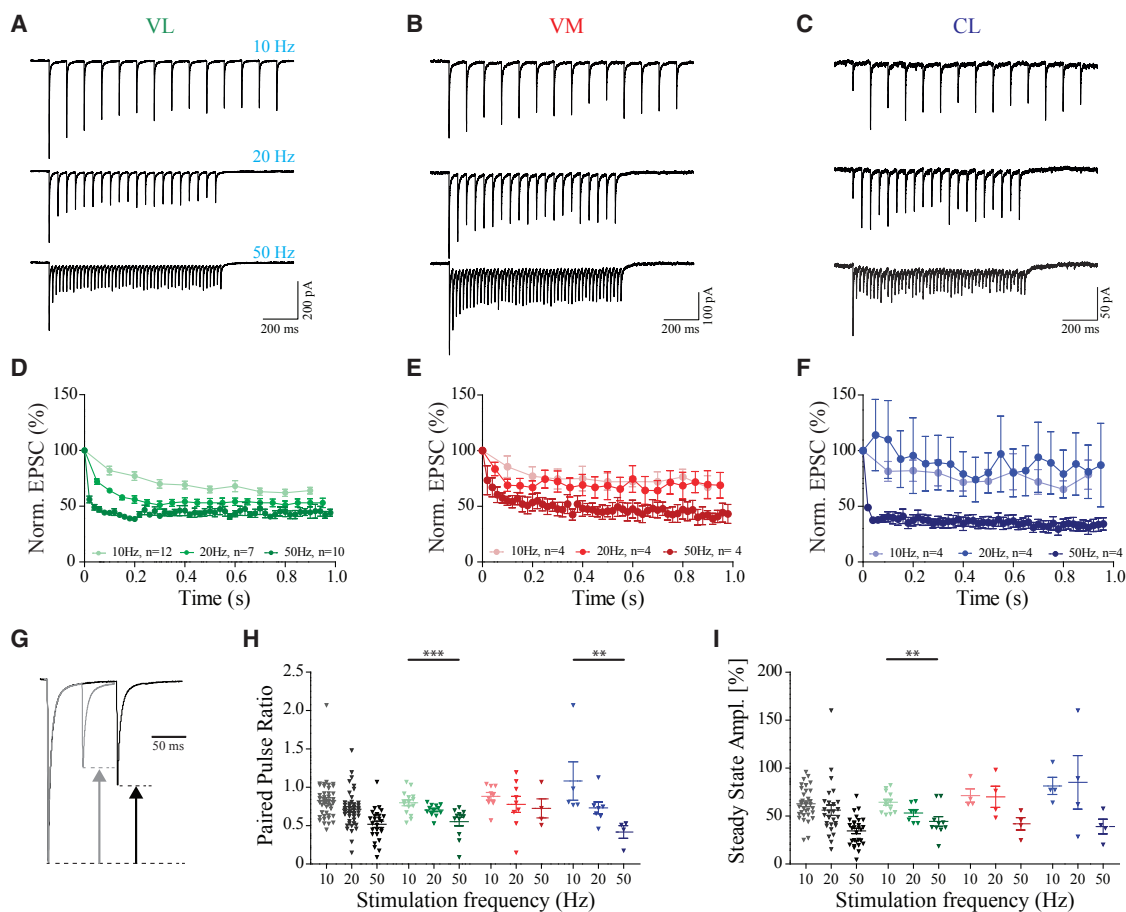


Figure 3. High-Frequency Stimulation Results in PPD of EPSC

(A–C) Averaged responses of VL (A), VM (B), and CL (C) neurons (of five repeats) to 1-s trains of 10-, 20-, or 50-Hz stimuli.

(D–F) Average normalized EPSC amplitudes recorded in VL (D), VM (E), and CL (F) evoked by 10-, 20-, and 50-Hz stimulus trains.

(G) Superimposed example responses (average of five repeats) to paired-pulse stimulation at 10 Hz (black) and 20 Hz (gray).

(H) Average paired-pulse ratio at 10, 20, and 50 Hz for each recorded cell in each nucleus.

(I) Average normalized steady-state response amplitude during the last five stimuli of the train for each cell in each nucleus. (For [H], VL, n = 39; VM, n = 22; CL, n = 16; and [I], VL, n = 29; VM, n = 12; CL, n = 12).

Data are presented as mean \pm SEM. **p < 0.01, ***p < 0.001. For full statistical report, see Table S3.

et al., 1998; Reichova and Sherman, 2004) did not affect the remaining current (-12.1 ± 3.9 nA \cdot ms; Friedman test, $p = 1$; Figure 4B; Table S4), suggesting the absence of a substantial mGluR1- or mGluR5-mediated component in cerebellar transmission on thalamic neurons.

Postsynaptic Determinants of Variable CN Impact in Thalamic Cells

Next, we evaluated whether the electrophysiological characteristics described above could be linked to the morphology of the thalamic neurons, bearing in mind that in rat thalamus the neuronal morphology in VL, VM, and CL neurons varies (Clascá et al., 2012; Deschênes et al., 1996a, 1996b; Kuramoto et al., 2009, 2015; Ohno et al., 2012; Rubio-Garrido et al., 2009). By reconstructing biocytin-filled neurons throughout the VL, VM, and CL nuclei (Figure 5A) and analyzing their dendritic branching using a 3D Sholl analysis (Figure 5B), we found

that 23 VL neurons on average show a more elaborate branching pattern than the 14 CL neurons at 55- μ m distance from the soma ($p < 0.05$, two-way ANOVA; Mann-Whitney comparison; Figures 5C and 5D; Table S5). The number of proximal dendrites (VL, 8.13 ± 0.47 ; VM, 7.83 ± 0.83 ; CL, 6.83 ± 0.34) was not significantly different between nuclei ($p = 0.115$, K-W test; Figure 5E; Table S5). To better illustrate the dendritic architecture of cells in each of the three defined nuclei, we also quantified the angular distance between dendrites at 15 μ m from the soma. We found no significant difference in the angular distance (VL, $40.2 \pm 2.6^\circ$; VM, $41.1 \pm 3.5^\circ$; CL, $47.0 \pm 2.8^\circ$; $p = 0.14$, K-W test; Figures 5F and 5G; Table S5). Although limited, these morphological distinctions between cerebellar-recipient neurons possibly corroborate the distinct electrophysiological characteristics, which together suggest a differential impact of cerebellar input to thalamic neurons.

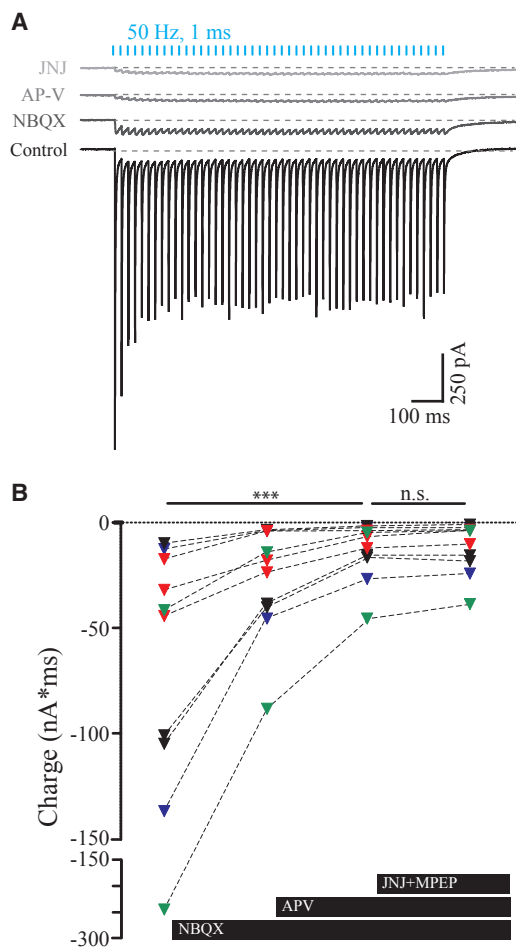


Figure 4. Thalamic Responses to CN Stimulation Are Sensitive to Ionotropic Receptor Blockers

(A) Example traces of averaged EPSCs evoked by 1-s train of 1-ms pulses at 50 Hz in control (aCSF) conditions and following application of NBQX, APV, and JNJ to block AMPA, NMDA, and mGluR1 and 5 receptors, respectively. (B) Summary data showing the decrease of charge after drug application (VL in green, VM in red, CL in blue, and undefined location in black; $n = 10$ in total). *** $p < 0.001$. For full statistical report, see Table S4.

Distribution and Morphology of Reconstructed CN Terminals

Previous structural studies in rats suggested that, in VL, cerebellar terminals are larger than those in IL nuclei (Aumann and Horne, 1996b). To further characterize the identity of cerebellar terminals for each recorded neuron, we stained the tissue slices containing the patched neurons for vGluT2 and assessed the morphology of the vGluT2⁺-CN terminals using high-magnification confocal microscopy (Figure 6A). The number of vGluT2⁺-CN terminals on the recorded cells did not vary significantly between the nuclei (VL, 4.5 ± 0.7 ; VM, 3.66 ± 1.17 ; CL, 3.08 ± 0.83 ; $p = 0.37$, K-W test; Figure 6C; Table S6), nor did their distance from soma (VL, $26.7 \pm 1.9 \mu\text{m}$; VM, $33.8 \pm 5.7 \mu\text{m}$; CL, $26.6 \pm 2.5 \mu\text{m}$; $p = 0.58$, K-W test; Figure 6D; Table S6). To enhance the x-y resolution and reduce the blurring caused by the point spread function, we deconvolved the images and

selected the virus-labeled vGluT2⁺-CN terminals to measure their volume (Figure 6B). We found that terminals onto recorded VL neurons had a larger volume ($11.67 \pm 1.30 \mu\text{m}^3$) than those onto recorded CL neurons (CL, $7.23 \pm 1.57 \mu\text{m}^3$) ($p = 0.02$, K-W test; Figures 6E and 6F; Table S6), whereas no significant differences were found comparing VM terminals ($9.26 \pm 1.93 \mu\text{m}^3$) to VL and CL ($p = 1.00$ and $p = 0.35$, respectively; K-W tests; Figures 6E and 6F; Table S6).

To further investigate CN axon terminal dimensions and characteristics of the postsynaptic structures, we studied synaptic contacts at the ultrastructural level. To identify CN axon terminals in electron micrographs, we collected VL, VM, and CL tissue from mice that we injected with biotin dextran amine (BDA) in CN, which spread mostly, but not exclusively, in the interposed CN. Representative examples of the synaptic profiles formed by BDA-stained CN terminals and thalamic neurons are shown in Figure 7A. Measurements made from the profiles included terminal surface, number and size of mitochondria, dendritic diameter, postsynaptic density (PSD) length, and number of release sites per terminal (Figure 7B). Although we observed in the fluorescent images that the terminal size was significantly different between VL and CL, at the ultrastructural level the difference was not significant even though on average VL terminals appeared to be bigger (VL, $n = 42$ terminals, $2.35 \pm 0.38 \mu\text{m}^2$; VM, $n = 27$ terminals, $2.07 \pm 0.31 \mu\text{m}^2$; CL, $n = 28$ terminals, $1.23 \pm 0.11 \mu\text{m}^2$; $p = 0.099$, K-W test). We did observe a significant difference in the mitochondrial surface between VL and CL (VL, $0.13 \pm 0.01 \mu\text{m}^2$; VM, $0.10 \pm 0.01 \mu\text{m}^2$; CL, $0.06 \pm 0.01 \mu\text{m}^2$; VL versus VM, $p = 0.034$; VL versus CL, $p < 0.001$; VM versus CL, $p < 0.001$; K-W test; Figure 7B; Table S7), which correlated significantly with the total surface of the terminals ($r_s = 0.7156$; $p < 0.001$, Spearman correlation; Figure 7C; Table S7). Another characteristic of cerebello-thalamic synapses we could observe in all three nuclei is that most terminals contained several release sites (VL, 2.97 ± 0.38 ; VM, 3.08 ± 0.47 ; CL, 2.96 ± 0.29 ; $p = 0.667$, K-W test) (Aumann et al., 1994). The axon terminals in VL and VM also showed a more complex interaction with the postsynaptic structures than in CL, in that we found dendritic protrusions inside the majority of the VL (24 out of 42 terminals) and VM (17 out of 27) terminals, whereas this was less common in CL (4 out of 28) terminals. No significant differences were found in the surface of the dendritic protrusions between the thalamic nuclei (VL, $0.23 \pm 0.16 \mu\text{m}^2$; VM, $0.29 \pm 0.18 \mu\text{m}^2$; CL, $0.13 \pm 0.12 \mu\text{m}^2$; $p = 0.172$, K-W test). The surface area of the dendritic protrusions showed a significant correlation with the terminals surface ($r_s = 0.6146$; $p < 0.001$, Spearman correlation; Figure 7C; Table S7). At the postsynaptic side, we found that although the dendritic diameter opposing CN terminals did not show any difference between the nuclei (VL, $0.97 \pm 0.13 \mu\text{m}$; VM, $1.18 \pm 0.12 \mu\text{m}$; CL, $0.84 \pm 0.08 \mu\text{m}$; $p = 0.08$, K-W test), we did find that the length of PSDs was longer in VL ($0.17 \pm 0.01 \mu\text{m}$) compared to VM ($0.14 \pm 0.01 \mu\text{m}$) and CL ($0.15 \pm 0.01 \mu\text{m}$; VL versus VM, $p = 0.024$; VL versus CL, $p = 0.055$; VM versus CL, $p = 1$; K-W test). Altogether, these ultrastructural findings support the notion that CN axons tend to synapse on proximal dendrites in all three studied nuclei, but that there may be a structural difference in the constellation of the presynaptic and postsynaptic sites that could correlate to

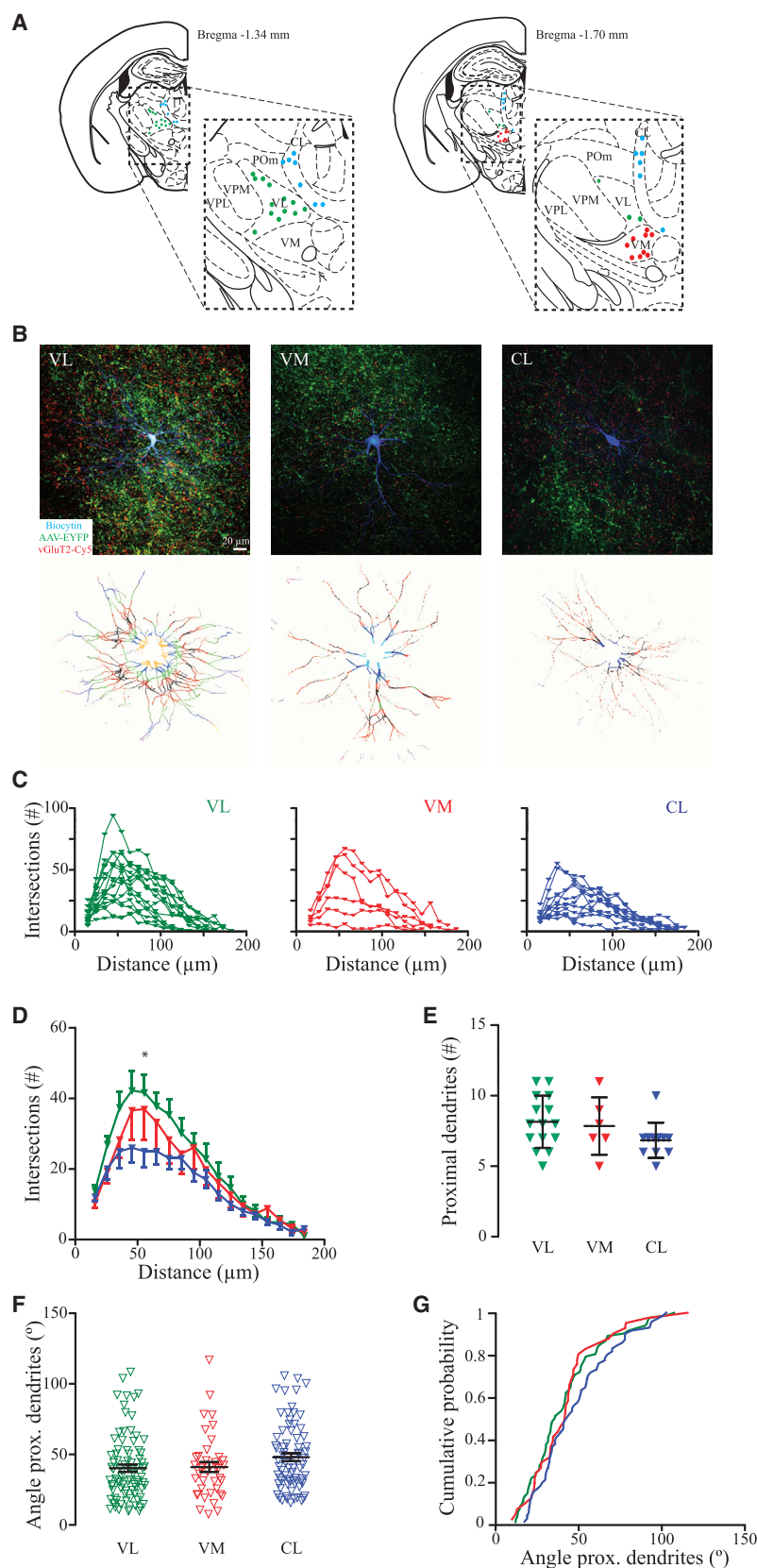


Figure 5. Morphological Characterization of Thalamic Cells Recorded in VL, VM, and CL

(A) Location of all recorded cells in VL, VM, and CL projected on two coronal planes (Franklin and Paxinos, 2001).

(B) Top: maximum projections of the somatodendritic morphology of biocytin-filled cells (blue), surrounding ChR2-EYFP-labeled CN axons (green) and vGluT2-staining (red) for VL (left), VM (middle), and CL (right). Bottom: maximum projections of 10- μm -thick 3D spheres surrounding an example neuron from VL, VM, and CL (as indicated by the different colors along dendritic trees).

(C) Sholl analysis shows dendritic arborization by the number of intersections of the concentric spheres for VL (left), VM (middle), and CL (right) (VL, $n = 15$; VM, $n = 6$; CL, $n = 11$).

(D) Average number of dendritic intersections is shown in 10- μm steps from the soma and each nucleus.

(E) Number of proximal dendrites as quantified at 15- μm distance from soma for VL ($n = 15$), VM ($n = 6$), and CL ($n = 11$).

(F) Directionality of proximal dendrites (at 15 μm from soma center) is determined by the angle between individual dendrites. Note that the angle is proportional to the angular distance between two neighboring dendrites.

(G) Cumulative distribution of data represented in (F). Data are presented as mean \pm SEM. * $p < 0.05$. For full statistical report, see Table S5.

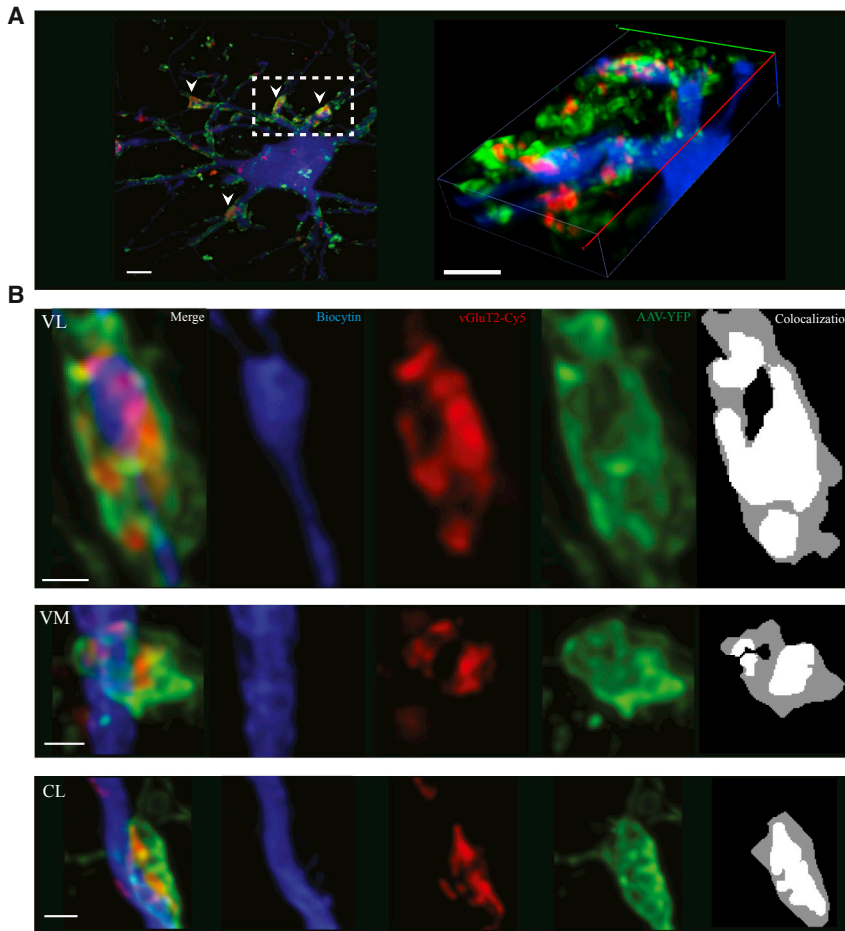


Figure 6. CN Terminals of Variable Volume Are Similarly Positioned along Dendrites of Recorded Thalamic Neurons

(A) Maximum-intensity projection of Z-stack image (22- μm thick) of biocytin-filled neuron (blue, streptavidin-Cy3; green, ChR2-YFP terminals; red, vGluT2-Cy5). Arrowheads indicate the vGluT2⁺-CN terminals onto proximal thalamic dendrites. Scale bar, 10 μm . Right: 3D reconstruction of inset in (A). Scale bar, 2.5 μm .

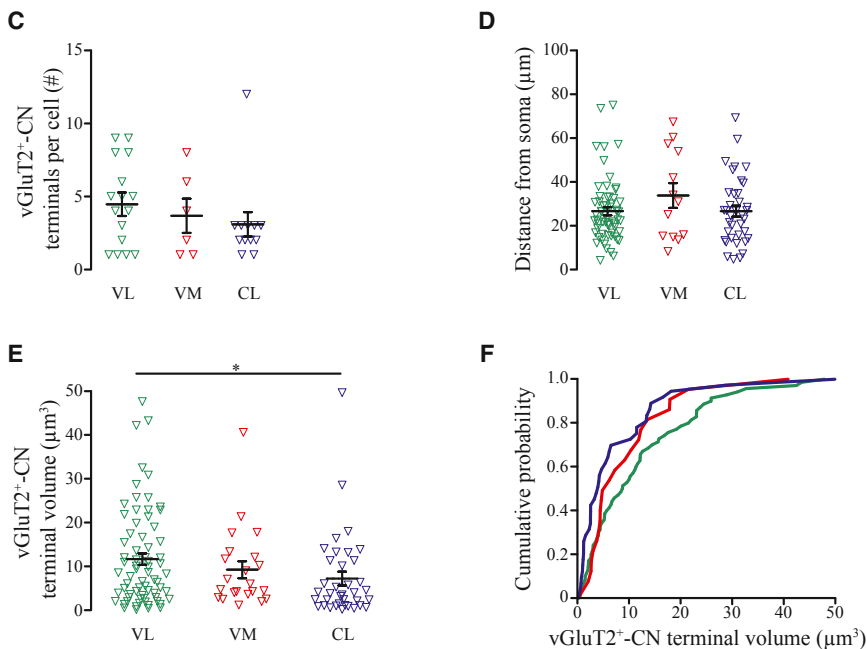
(B) Left four panels: example of vGluT2⁺-CN terminals in VL, VM and CL (blue, thalamic dendrite; red, vGluT2; green, CN terminal). Right: colocalization of ChR2-EYFP and vGluT2 staining to identify active terminals and calculate their volume based on ChR2-EYFP signal. Scale bar, 1 μm .

(C) Summary data of the number of reconstructed vGluT2⁺-CN terminals (VL, n = 16; VM, n = 6; CL, n = 12).

(D) Summary data of distance of reconstructed terminals from soma (VL, n = 60; VM, n = 13; CL, n = 37).

(E and F) Terminal volume (VL, n = 71; VM, n = 22; CL, n = 37) (E) and cumulative distribution (F).

Data are presented as mean \pm SEM. *p < 0.05. For full statistical report, see Table S6.



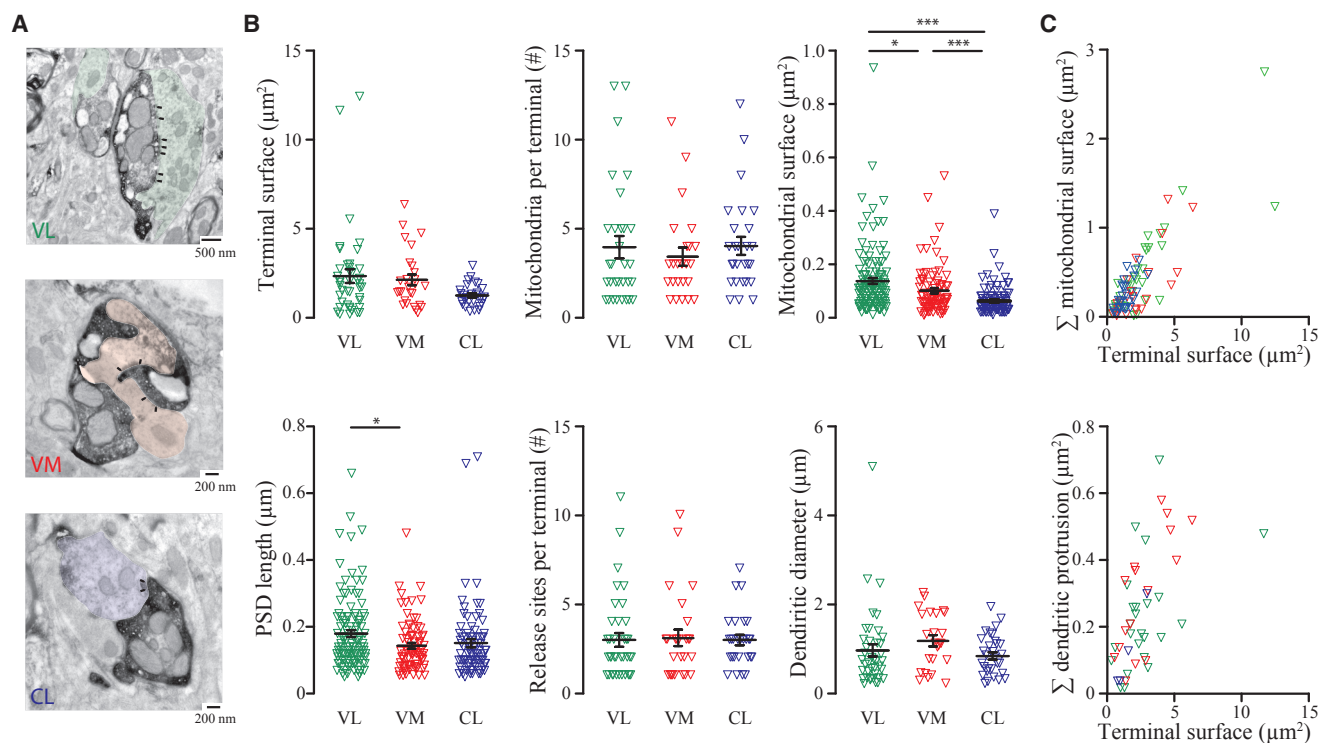


Figure 7. Ultrastructure of CN Terminals in VL, VM, and CL Reveals Presynaptic and Postsynaptic Specialization

(A) Pseudo-colored ultramicrographs of CN terminal in VL (top), VM (middle), and CL (bottom). Note the complex structure of these terminals. Arrowheads indicate synapses.

(B) Quantification of terminal surface (top left; VL, n = 48; VM, n = 28; CL, n = 27), number of mitochondria (top middle; VL, n = 32; VM, n = 27; CL, n = 24), mitochondrial surface (top right; VL, n = 124; VM, n = 109; CL, n = 82; VL versus VM, $p = 0.034$; VL versus CL, $p < 0.001$; VM versus CL, $p < 0.001$, K-W tests), length of postsynaptic density (PSD) (bottom left; VL, n = 114; VM, n = 81; CL, n = 80; VL versus VM, $p = 0.024$; VL versus CL, $p = 0.055$; VM versus CL, $p = 1$; K-W test), release sites per terminal (bottom middle; VL, n = 37; VM, n = 27; CL, n = 26; $p = 0.667$, K-W test), and diameter of the contacted dendrite (bottom right; VL, n = 40; VM, n = 31; CL, n = 25; $p = 0.080$, K-W test).

(C) Top: correlation of the terminal surface with the sum of the surface occupied by mitochondria for each given terminal (VL, green; VM, red; CL, blue). Bottom: correlation of the terminal surface with the sum of the surface occupied by dendritic protrusions for each given terminal. Note that terminals without a mitochondria or dendritic protrusion are not represented in these correlation plots.

Data are presented as mean \pm SEM. * $p < 0.05$; *** $p < 0.001$. For full statistical report, see [Table S7](#).

the difference in transmission at CN-synapses throughout the thalamic complex.

DISCUSSION

Our data show that, in mouse brain, CN neurons innervate the VL thalamic nucleus more densely compared to VM and CL. Although the distribution matches that in other species ([Angaut et al., 1985](#); [Asanuma et al., 1983](#); [Aumann and Horne, 1996b](#); [Aumann et al., 1994](#); [Bentivoglio and Kuypers, 1982](#); [Cohen et al., 1958](#); [Haroian et al., 1981](#); [Teune et al., 2000](#)), our study does provide a quantitative comparison of active CN axon terminals in VL, VM, and CL, since we exclusively quantified the vGluT2⁺-CN terminals that expressed ChR2-EYFP. Our density values of these CN terminals per nucleus ([Figure 1](#)) may very well be an underestimate of the total proportion of CN axons that innervate VL, VM, and CL nuclei given that (1) the injections of viral particles did not transfect the complete CN population projecting to these nuclei and (2) the use of vGluT2 antibodies

most likely resulted in a limited penetrance into the slices, leaving those ChR2-expressing CN terminals located deeper into the slice unstained. These aspects possibly also confounded the number and location of CN axon terminals on a single thalamic neuron ([Figure 6](#)) in that there may have been more CN terminals that contributed to the evoked charge transfer, but that due to their location, i.e., depth in the slice, some were identified as vGluT2-negative. Still, we would like to emphasize that the difference in the number of CN terminals between VL, VM, and CL is likely to be independent from viral transfection rates or antibody penetrance since these data have been gathered from the same tissue samples.

A potential source for the variability of CN-evoked responses in thalamic neurons and the difference in CN-terminal morphology throughout the thalamic nuclei may be the location of the transfected CN neurons. According to previous anatomical studies that used classical neurotracers, glutamatergic projection neurons from the lateral, interposed, and medial CN all innervate VL, VM, and CL neurons with a clear preference

for the contralateral thalamic complex, but not excluding ipsilateral projections (Angaut et al., 1985; Haroian et al., 1981; Teune et al., 2000). Whereas we aimed for centering our bilateral viral injections in the interposed nuclei, we also found ChR2-EYFP transfected CN neurons in the lateral and/or medial CN in several mice. Although in principle it is possible that the variability in the recorded responses and terminal morphology is due to the transfection of glutamatergic CN neurons in various nuclei in both sides of the cerebellum, there are currently no data available supporting such a notion. In fact, the few data available on the direct comparison between axon terminals from the various nuclei reveal that the dimensions and ultrastructural morphology in thalamic nuclei is comparable between axons originating from interposed and lateral CN (Aumann et al., 1994). These anatomical data are corroborated by the previous *in vivo* electrophysiological experiments using intracellular and extracellular recordings in anesthetized cats that revealed that electrical stimulation of both the interposed and lateral CN can evoke postsynaptic responses in single VL thalamic neurons (Bava et al., 1986; Rispal-Padel and Grangetto, 1977; Shinoda et al., 1985; Smith et al., 1978; Uno et al., 1970). A set of dedicated *in vitro* experiments using tissue with small injections in the single CN will provide further insight in the potential role of the various CN in the differentiation of the cerebellar impact on thalamic nuclei.

The electrophysiological characterization of thalamic responses to CN stimulation revealed that, on average, VL neurons showed larger EPSCs than those in VM or CL. As expected, these voltage-clamp results translated to a higher chance of action potential firing upon stimulation for VL than for VM and CL when recorded in current clamp. Our data from VL and VM match earlier reports about faithful action potential firing by VL neurons upon CN or brachium conjunctivum stimulation (Bava et al., 1986; Rispal-Padel and Grangetto, 1977; Sawyer et al., 1994b; Steriade, 1995; Steriade et al., 1971; Uno et al., 1970) and provide detailed insights for synaptic transmission at CN-CL synapses (cf. Bava et al., 1967; Chen et al., 2014). Using 10-, 20-, and 50-Hz stimulus trains, we were able to sample the responses of thalamic neurons to physiologically relevant cerebellar input, since the firing rates reported for CN projections recorded *in vivo* range from ~30 to 100 Hz (as reviewed by De Zeeuw et al., 2011). We consistently found that the responses in VL, VM, and CL neurons showed PPD, which is suggested to play an important role in information processing by helping the system to adapt to ongoing levels of activity (Chung et al., 2002; Mease et al., 2014; Reichova and Sherman, 2004). In our current experiments, the ChR2 off-kinetics limited us to stimulus frequencies well below the maximal CN firing rates, which may also have prevented us from recording a significant effect of mGluR-receptor blockage, in that the total mGluR-mediated currents in thalamic neurons evoked by a stimulus frequency of 50 Hz tends to be limited (see also Viaene et al., 2013). Therefore, we cannot rule out that the activation of either presynaptic or postsynaptic modulatory mechanisms have affected the responses we recorded *in vitro*.

Referring to intracellular *in vivo* recordings, the cerebellar input on VL neurons has been classified as a driver input to neurons in the motor domain of the thalamus (Sawyer et al., 1994b; Sher-

man, 2014; Uno et al., 1970). However, several recent papers classify thalamic inputs in more than two categories: in addition to the “driver” and “modulator” inputs, a third category of “driver-like” input has been defined (Bickford, 2016; Bickford et al., 2015). In the tecto-geniculate system, the driver-like inputs have also been identified at the anatomical level by medium-sized terminals that contain round vesicles and innervate proximal dendrites, and at the electrophysiological level stable response amplitudes to trains of stimuli of up to 20 Hz (Kelly et al., 2003; Masterson et al., 2009). Our *in vitro* data showed that responses in VL neurons to stimulation of CN terminals meet a number of criteria used to define driver inputs (Sherman and Guillery, 1998): (1) CN stimulation evokes a large postsynaptic current that (2) is solely mediated by ionotropic receptors and (3) depresses upon higher-frequency stimulation; (4) CN axons form large synaptic boutons that (5) contact proximal thalamic dendrites. For CN terminals in VM and CL, the categorization is less clear, since these only show some of the driver characteristics. They lack mGluR-mediated transmission and proximal terminal location and their terminal volume is smaller. Moreover, the responses of VM and CL neurons to CN stimulation are significantly smaller, and CL neurons tend to show a stable paired-pulse ratio in response to 10-Hz stimulus trains. At the ultrastructural level, we also found a trend, although not significant, to a reduced terminal surface in CL compared to VL and a significantly smaller CL mitochondrial surface. Given that previous studies revealed that terminals with larger surface have a higher chance to release neurotransmitter compared to smaller terminals (Rollenhagen and Lübke, 2006; Zikopoulos and Barbas, 2007, 2012), our data may at least partially explain why the evoked response amplitude and charge in CL were smaller and more variable (Figure 2).

Further explanation for the difference in postsynaptic responses to CN stimulation between VL and the other nuclei may come from the difference in PSD length, which previously has been linked to neurotransmission efficacy (Geinisman, 1993). Our ultrastructural analysis of CN terminals further revealed that the characteristics described earlier for VL in the rat brain, i.e., large terminal surface, presence of multiple mitochondria, fragmented release sites, and large diameter of opposing dendritic structure (Aumann and Horne, 1996a; Aumann et al., 1994; Sawyer et al., 1994a), are also found in mouse brain. The complexity of the cerebello-thalamic contacts in the VL and VM seemed more prominent, in that CN terminals in these nuclei were found to contain dendritic protrusions more often than in CL. This typical structure, found also in other large terminals in thalamus, such as those formed by the piriform cortex in medial thalamus (Pelzer et al., 2017), enlarge the contact surface between axon terminals and the dendrite. However, in our current dataset, we found no significant difference between the number of release sites for VL, VM, or CL. Future experiments on the release properties of single CN terminals, alike those performed for “giant” corticothalamic synapses in the sensory system (Groh et al., 2008; Seol and Kuner, 2015), should elucidate how the morphological characteristics can translate into the clear differentiation between postsynaptic responses in VL, VM, and CL.

Our current findings provide building blocks to construct the frame of reference for the impact of the cerebellar output on thalamic neurons. Given that mouse thalamus VL, VM, and CL are free of interneurons, we argue that all our recordings are from thalamic relay neurons that synapse throughout the various regions of the cerebral cortex. By adapting the classification of relay neurons from rat thalamus (reviewed by [Clascá et al., 2012](#)), our VL recordings are from a mix of core (C)-type and matrix (M)-type neurons, VM recordings are from M-type neurons, and CL recordings are from IL-type neurons, which to some extent is supported by the reduced dendritic branching of CL neurons ([Figure 6](#)). If we assume that the axonal branching of C, M, and IL neurons in mouse brain indeed shows lamina-specific termination as described for rat ([Deschênes et al., 1996b](#); [Herkenham, 1979, 1980](#); [Kuramoto et al., 2009, 2015](#)), our data indicate that the information conveyed by C- and M-type neurons in VL to manipulate activity of the middle and output layers of motor cortices ([Kuramoto et al., 2009](#)) that contribute to initiation of movement ([Goldberg et al., 2013](#)). In contrast, M-type VM neurons projections are more dense in layer 1 of widespread cortical areas, including the motor-associated, orbital, cingulate, and visual areas in the rat ([Kuramoto et al., 2015](#)). Direct activation of cerebellar afferents to VM neurons indeed resulted in a widespread change of cortical activity to the gamma-band range ([Steriade, 1995](#)), which in these VM-projection regions have been linked to cognitive processes. Indeed, a recent study indicates that the cerebellar-recipient zone in mouse VM has a reciprocal connection with the prefrontal anterior lateral motor cortex that determines the ability to prepare a correct motor response to a sensory cue ([Guo et al., 2017](#)). For IL-type CL neurons, it has been shown that their axons excite striatal, but also cortical neurons affecting motor, pre-motor, parietal, prefrontal, and anterior cingulate processing, as well as regulating behavioral arousal levels ([Berendse and Groenewegen, 1991](#); [Chen et al., 2014](#); [Gummadavelli et al., 2015](#)).

Although it remains to be investigated how *in vivo* conditions thalamic responses may differ between the different types of neurons, our study provides insights into the diversity of the cerebellar impact on thalamo-cortical networks. Thalamo-cortical activity exhibits two distinct states, i.e., tonic and burst firing, which are related to different conditions such as waking, non-rapid eye movement (REM) state, slow-wave sleep, or even epileptogenic activity ([McCormick and Bal, 1997](#)). Thalamic afferents, like CN axons, are likely to modulate the activity of thalamo-cortical relay neurons from tonic to burst firing and vice versa. Indeed, single-pulse stimulation of CN neurons efficiently stops thalamo-cortical oscillations in epileptic mutant mice ([Kros et al., 2015](#)). The underlying mechanism may at least partially depend on the variable impact of CN axons on thalamic neurons, as we showed for VL, VM, and CL. For instance, a brief pause in the firing of CN neurons, which can occur following synchronized activity in the cerebellar cortex ([De Zeeuw et al., 2011](#)), will most likely result in a recovery of synaptic PPD for all nuclei, but the first postsynaptic response in VL will be notably larger than in VM or CL. Such differential effects on thalamic action potential firing may potentially be modulated by cortical input,

as well as glycinergic or cholinergic projections arising from brainstem ([Giber et al., 2015](#); [Miller et al., 1992](#)) or GABAergic projections from substantia nigra ([Buee et al., 1986](#)), all of which may synergistically diversify the cerebellar impact on thalamo-cortical processes throughout the various (non-)motor domains.

EXPERIMENTAL PROCEDURES

Animals

All experiments were performed in accordance with the European Communities Council Directive. Protocols were reviewed and approved by the Dutch National Experimental Animal Committees (DEC), and every precaution was taken to minimize stress, discomfort, and the number of animals used. Data were collected from 21- to 56-day-old C57BL/6NHsd mice of both sexes, which were purchased from Envigo Laboratories (Horst, The Netherlands).

Virus Injections

We performed stereotaxic injections of adeno-associated virus carrying Channelrhodopsin2 AAV2-hSyn-ChR2(H134R)-EYFP into CN at 2 mm anterior-posterior and 1.5–2 mm medial-lateral to lambda. For localization of the injection sites, 40- μ m-thick horizontal sections were obtained on a freezing microtome. The tissue was incubated with DAPI (300 nM). Sections were rinsed and mounted on glass.

Electrophysiological Recordings in Slices and Optogenetics

Electrophysiological recordings in coronal or horizontal slices were performed at $34 \pm 1^\circ\text{C}$ in artificial cerebrospinal fluid (aCSF) 40 min after dissection. Internal solution was supplemented with biocytin for morphological reconstruction. Full-field optogenetic stimulation (1 ms, 470-nm peak excitation, 0.1–6.65 mW/mm²) was generated using a Polygon4000 (Mightex, Toronto, ON, Canada) or a pE2 (CoolLED, Andover, UK). Pharmacology experiments were assessed adding AMPA (10 μ M NBQX), NMDA (10 μ M APV), mGluR1 (10 μ M JNJ-16259685), and mGluR5 (50 μ M MPEP) blockers to the aCSF.

Immunofluorescence and Reconstruction

To visualize the recorded neurons and CN terminals, slices were stained for streptavidin-Cy3 (Jackson ImmunoResearch) and vGluT2 anti-guinea pig Cy5 (Millipore Bioscience Research reagent). Using custom-written Fiji-scripts (ImageJ), we identified putative synaptic contacts that were isolated and morphologically studied using a LSM 700 microscope (Carl Zeiss). Stack's subsets of the connection were deconvolved using Huygens software (Scientific Volume Imaging), and the volume was measured using a custom-written Fiji macro. To quantify the distance from soma for vGluT2-positive CN terminals, we calculated the distance in three dimensions (using x-, y-, z-coordinates) between the center of the terminal and the center of the soma by Pythagorean theorem. To determine the dendritic arborization of biocytin-filled cells, we used the 3D Sholl analysis macro implemented in Fiji software ([Ferreira et al., 2014](#)).

Electron Microscopy

Ultrastructural morphology was analyzed using electron microscope (CM 100; Philips). Staining for diaminobenzidine (DAB) and preparation of ultrathin section were performed as previously described ([Hoebeek et al., 2008](#)).

Data Analysis and Statistics

All numerical values are given as means, and error bars are SEM. Parametric and non-parametric tests were chosen as appropriate and were reported in figure legends. Data analyses were performed using SPSS 22.0 software package.

Detailed experimental procedures and statistical analyses for each experiment can be found in [Supplemental Experimental Procedures](#).

SUPPLEMENTAL INFORMATION

Supplemental Information includes Supplemental Experimental Procedures and seven tables and can be found with this article online at <https://doi.org/10.1016/j.celrep.2018.04.098>.

ACKNOWLEDGMENTS

We thank Daniel Dumas, Bas van Hoogstraten, Sverrir V. Sigurdsson, Farnaz Nassirinia, Valentina Riguccini, Elena Tiddens, Saša Peter, Negah Rahmati, Avi Libster, Martijn Sierksma, Federica Brunero, and all other members of the Hoebeek group for fruitful scientific discussions. We kindly thank Erika H. Sabel-Goedknegt, Elize D. Haasdijk, Patrick Eikenboom, and the OIC group for expert assistance in immunohistochemistry and/or imaging. S.V.G., C.B.S., O.H.J.E.R., and F.E.H. are generously supported by the Dutch Organization for Life Sciences (NWO-ALW VIDI 016.121.346 and Zon-MW TOP GO 91210067 to F.E.H.), and C.I.D.Z. by ERC-Adv (294775), ERC-PoC (768914), NWO-ALW (854.10.004), and Zon-MW (91210067) grants.

AUTHOR CONTRIBUTIONS

S.V.G. performed and analyzed the *in vitro* electrophysiological recordings, the confocal image acquisition, and digital reconstructions. C.B.S. performed electrophysiological recordings and analysis and designed and performed Sholl analysis. O.H.J.E.R. performed channelrhodopsin and BDA injections for *in vitro* recordings and EM analysis. A.N. developed image analysis scripts and provided technical support for image acquisition. C.I.D.Z. and F.E.H. contributed financial and technical support. S.V.G. and F.E.H. wrote the original draft. C.I.D.Z. and C.B.S. edited the manuscript. F.E.H. conceived and guided the project and performed ultrastructural analysis.

DECLARATIONS OF INTERESTS

The authors declare no competing interests.

Received: October 19, 2017

Revised: February 26, 2018

Accepted: April 24, 2018

Published: May 29, 2018

REFERENCES

- Angaut, P., Cicirata, F., and Serapide, F. (1985). Topographic organization of the cerebellothalamic projections in the rat. An autoradiographic study. *Neuroscience* 15, 389–401.
- Asanuma, C., Thach, W.T., and Jones, E.G. (1983). Distribution of cerebellar terminations and their relation to other afferent terminations in the ventral lateral thalamic region of the monkey. *Brain Res.* 286, 237–265.
- Aumann, T.D., and Horne, M.K. (1996a). A comparison of the ultrastructure of synapses in the cerebello-rubral and cerebello-thalamic pathways in the rat. *Neurosci. Lett.* 211, 175–178.
- Aumann, T.D., and Horne, M.K. (1996b). Ramification and termination of single axons in the cerebellothalamic pathway of the rat. *J. Comp. Neurol.* 376, 420–430.
- Aumann, T.D., Rawson, J.A., Finkelstein, D.I., and Horne, M.K. (1994). Projections from the lateral and interposed cerebellar nuclei to the thalamus of the rat: a light and electron microscopic study using single and double anterograde labelling. *J. Comp. Neurol.* 349, 165–181.
- Bava, A., Manzoni, T., and Urbano, A. (1967). Effects of fastigial stimulation on thalamic neurones belonging to the diffuse projection system. *Brain Res.* 4, 378–380.
- Bava, A., Cicirata, F., Giuffrida, R., Licciardello, S., and Panto, M.R. (1986). Electrophysiologic properties and nature of ventrolateral thalamic nucleus neurons reactive to converging inputs of paleo- and neocerebellar origin. *Exp. Neurol.* 91, 1–12.
- Bentivoglio, M., and Kuypers, H.G. (1982). Divergent axon collaterals from rat cerebellar nuclei to diencephalon, mesencephalon, medulla oblongata and cervical cord. A fluorescent double retrograde labeling study. *Exp. Brain Res.* 46, 339–356.
- Berendse, H.W., and Groenewegen, H.J. (1991). Restricted cortical termination fields of the midline and intralaminar thalamic nuclei in the rat. *Neuroscience* 42, 73–102.
- Bickford, M.E. (2016). Thalamic circuit diversity: modulation of the driver/modulator framework. *Front. Neural Circuits* 9, 86.
- Bickford, M.E., Zhou, N., Krahe, T.E., Govindaiah, G., and Guido, W. (2015). Retinal and tectal “driver-like” inputs converge in the shell of the mouse dorsal lateral geniculate nucleus. *J. Neurosci.* 35, 10523–10534.
- Bodranghien, F., Bastian, A., Casali, C., Hallett, M., Louis, E.D., Manto, M., Mariën, P., Nowak, D.A., Schmahmann, J.D., Serrao, M., et al. (2016). Consensus paper: revisiting the symptoms and signs of cerebellar syndrome. *Cerebellum* 15, 369–391.
- Brooks, J.X., Carriot, J., and Cullen, K.E. (2015). Learning to expect the unexpected: rapid updating in primate cerebellum during voluntary self-motion. *Nat. Neurosci.* 18, 1310–1317.
- Buee, J., Deniau, J.M., and Chevalier, G. (1986). Nigral modulation of cerebello-thalamo-cortical transmission in the ventral medial thalamic nucleus. *Exp. Brain Res.* 65, 241–244.
- Chen, C.H., Fremont, R., Arteaga-Bracho, E.E., and Khodakhah, K. (2014). Short latency cerebellar modulation of the basal ganglia. *Nat. Neurosci.* 17, 1767–1775.
- Chung, S., Li, X., and Nelson, S.B. (2002). Short-term depression at thalamocortical synapses contributes to rapid adaptation of cortical sensory responses in vivo. *Neuron* 34, 437–446.
- Clascá, F., Rubio-Garrido, P., and Jabaudon, D. (2012). Unveiling the diversity of thalamocortical neuron subtypes. *Eur. J. Neurosci.* 35, 1524–1532.
- Cohen, D., Chambers, W.W., and Sprague, J.M. (1958). Experimental study of the efferent projections from the cerebellar nuclei to the brainstem of the cat. *J. Comp. Neurol.* 109, 233–259.
- Daniel, H., Billard, J.M., Angaut, P., and Batini, C. (1987). The interposito-rubrospinal system. Anatomical tracing of a motor control pathway in the rat. *Neurosci. Res.* 5, 87–112.
- De Zeeuw, C.I., and Ten Brinke, M.M. (2015). Motor learning and the cerebellum. *Cold Spring Harb. Perspect. Biol.* 7, a021683.
- De Zeeuw, C.I., Hoebeek, F.E., Bosman, L.W., Schonewille, M., Witter, L., and Koekkoek, S.K. (2011). Spatiotemporal firing patterns in the cerebellum. *Nat. Rev. Neurosci.* 12, 327–344.
- Deschênes, M., Bourassa, J., Doan, V.D., and Parent, A. (1996a). A single-cell study of the axonal projections arising from the posterior intralaminar thalamic nuclei in the rat. *Eur. J. Neurosci.* 8, 329–343.
- Deschênes, M., Bourassa, J., and Parent, A. (1996b). Striatal and cortical projections of single neurons from the central lateral thalamic nucleus in the rat. *Neuroscience* 72, 679–687.
- Ferreira, T.A., Blackman, A.V., Oyrer, J., Jayabal, S., Chung, A.J., Watt, A.J., Sjöström, P.J., and van Meyel, D.J. (2014). Neuronal morphometry directly from bitmaps images. *Nat. Methods* 11, 982–984.
- Franklin, K., and Paxinos, G. (2001). *The Mouse Brain in Stereotaxic Coordinates*, Compact, Second Edition (Academic Press).
- Geinisman, Y. (1993). Perforated axospinous synapses with multiple, completely partitioned transmission zones: probable structural intermediates in synaptic plasticity. *Hippocampus* 3, 417–433.
- Giber, K., Diana, M.A., Plattner, V., Dugué, G.P., Bokor, H., Rousseau, C.V., Maglóczy, Z., Havas, L., Hangya, B., Wildner, H., et al. (2015). A subcortical inhibitory signal for behavioral arrest in the thalamus. *Nat. Neurosci.* 18, 562–568.
- Goldberg, J.H., Farries, M.A., and Fee, M.S. (2013). Basal ganglia output to the thalamus: still a paradox. *Trends Neurosci.* 36, 695–705.

- Groh, A., de Kock, C.P., Wimmer, V.C., Sakmann, B., and Kuner, T. (2008). Driver or coincidence detector: modal switch of a corticothalamic giant synapse controlled by spontaneous activity and short-term depression. *J. Neurosci.* 28, 9652–9663.
- Gummadavelli, A., Motelow, J.E., Smith, N., Zhan, Q., Schiff, N.D., and Blumenfeld, H. (2015). Thalamic stimulation to improve level of consciousness after seizures: evaluation of electrophysiology and behavior. *Epilepsia* 56, 114–124.
- Guo, Z.V., Inagaki, H.K., Daie, K., Druckmann, S., Gerfen, C.R., and Svoboda, K. (2017). Maintenance of persistent activity in a frontal thalamocortical loop. *Nature* 545, 181–186.
- Harioian, A.J., Massopust, L.C., and Young, P.A. (1981). Cerebellothalamic projections in the rat: an autoradiographic and degeneration study. *J. Comp. Neurol.* 197, 217–236.
- Herkenham, M. (1979). The afferent and efferent connections of the ventromedial thalamic nucleus in the rat. *J. Comp. Neurol.* 183, 487–517.
- Herkenham, M. (1980). Laminar organization of thalamic projections to the rat neocortex. *Science* 207, 532–535.
- Hoebek, F.E., Khosrovani, S., Witter, L., and De Zeeuw, C.I. (2008). Purkinje cell input to cerebellar nuclei in tottering: ultrastructure and physiology. *Cerebellum* 7, 547–558.
- Jones, E.G. (1998). Viewpoint: the core and matrix of thalamic organization. *Neuroscience* 85, 331–345.
- Jones, E.G., and Hendry, S.H. (1989). Differential calcium binding protein immunoreactivity distinguishes classes of relay neurons in monkey thalamic nuclei. *Eur. J. Neurosci.* 1, 222–246.
- Kelly, L.R., Li, J., Carden, W.B., and Bickford, M.E. (2003). Ultrastructure and synaptic targets of tectothalamic terminals in the cat lateral posterior nucleus. *J. Comp. Neurol.* 464, 472–486.
- Kros, L., Eelkman Rooda, O.H., Spanke, J.K., Alva, P., van Dongen, M.N., Karpatis, A., Tolner, E.A., Strydis, C., Davey, N., Winkelman, B.H., et al. (2015). Cerebellar output controls generalized spike-and-wave discharge occurrence. *Ann. Neurol.* 77, 1027–1049.
- Kuramoto, E., Furuta, T., Nakamura, K.C., Unzai, T., Hioki, H., and Kaneko, T. (2009). Two types of thalamocortical projections from the motor thalamic nuclei of the rat: a single neuron-tracing study using viral vectors. *Cereb. Cortex* 19, 2065–2077.
- Kuramoto, E., Ohno, S., Furuta, T., Unzai, T., Tanaka, Y.R., Hioki, H., and Kaneko, T. (2015). Ventral medial nucleus neurons send thalamocortical afferents more widely and more preferentially to layer 1 than neurons of the ventral anterior-ventral lateral nuclear complex in the rat. *Cereb. Cortex* 25, 221–235.
- Liu, X.B., Muñoz, A., and Jones, E.G. (1998). Changes in subcellular localization of metabotropic glutamate receptor subtypes during postnatal development of mouse thalamus. *J. Comp. Neurol.* 395, 450–465.
- Manto, M., Bower, J.M., Conforto, A.B., Delgado-García, J.M., da Guarda, S.N., Gerwig, M., Habas, C., Hagura, N., Ivry, R.B., Mariën, P., et al. (2012). Consensus paper: roles of the cerebellum in motor control—the diversity of ideas on cerebellar involvement in movement. *Cerebellum* 11, 457–487.
- Masterson, S.P., Li, J., and Bickford, M.E. (2009). Synaptic organization of the tectorecipient zone of the rat lateral posterior nucleus. *J. Comp. Neurol.* 515, 647–663.
- McCormick, D.A., and Bal, T. (1997). Sleep and arousal: thalamocortical mechanisms. *Annu. Rev. Neurosci.* 20, 185–215.
- Mease, R.A., Krieger, P., and Groh, A. (2014). Cortical control of adaptation and sensory relay mode in the thalamus. *Proc. Natl. Acad. Sci. USA* 111, 6798–6803.
- Miller, J.W., Gray, B.C., and Bardgett, M.E. (1992). Characterization of cholinergic regulation of seizures by the midline thalamus. *Neuropharmacology* 31, 349–356.
- Monconduit, L., and Villanueva, L. (2005). The lateral ventromedial thalamic nucleus spreads nociceptive signals from the whole body surface to layer I of the frontal cortex. *Eur. J. Neurosci.* 21, 3395–3402.
- Ohno, S., Kuramoto, E., Furuta, T., Hioki, H., Tanaka, Y.R., Fujiyama, F., Sonomura, T., Uemura, M., Sugiyama, K., and Kaneko, T. (2012). A morphological analysis of thalamocortical axon fibers of rat posterior thalamic nuclei: a single neuron tracing study with viral vectors. *Cereb. Cortex* 22, 2840–2857.
- Pelzer, P., Horstmann, H., and Kuner, T. (2017). Ultrastructural and functional properties of a giant synapse driving the piriform cortex to mediodorsal thalamus projection. *Front. Synaptic Neurosci.* 9, 3.
- Peter, S., Ten Brinke, M.M., Stedehouder, J., Reinelt, C.M., Wu, B., Zhou, H., Zhou, K., Boele, H.J., Kushner, S.A., Lee, M.G., et al. (2016). Dysfunctional cerebellar Purkinje cells contribute to autism-like behaviour in Shank2-deficient mice. *Nat. Commun.* 7, 12627.
- Popa, D., Spolidoro, M., Proville, R.D., Guyon, N., Belliveau, L., and Léna, C. (2013). Functional role of the cerebellum in gamma-band synchronization of the sensory and motor cortices. *J. Neurosci.* 33, 6552–6556.
- Proville, R.D., Spolidoro, M., Guyon, N., Dugué, G.P., Selimi, F., Isope, P., Popa, D., and Léna, C. (2014). Cerebellum involvement in cortical sensorimotor circuits for the control of voluntary movements. *Nat. Neurosci.* 17, 1233–1239.
- Reichova, I., and Sherman, S.M. (2004). Somatosensory corticothalamic projections: distinguishing drivers from modulators. *J. Neurophysiol.* 92, 2185–2197.
- Rispal-Padel, L., and Grangetto, A. (1977). The cerebello-thalamo-cortical pathway. Topographical investigation at the unitary level in the cat. *Exp. Brain Res.* 28, 101–123.
- Rispal-Padel, L., and Latreille, J. (1974). The organization of projections from the cerebellar nuclei to the contralateral motor cortex in the cat. *Exp. Brain Res.* 19, 36–60.
- Rollenhagen, A., and Lübke, J.H. (2006). The morphology of excitatory central synapses: from structure to function. *Cell Tissue Res.* 326, 221–237.
- Rovó, Z., Ulbert, I., and Acsády, L. (2012). Drivers of the primate thalamus. *J. Neurosci.* 32, 17894–17908.
- Rubio-Garrido, P., Pérez-de-Manzo, F., Porrero, C., Galazo, M.J., and Clascá, F. (2009). Thalamic input to distal apical dendrites in neocortical layer 1 is massive and highly convergent. *Cereb. Cortex* 19, 2380–2395.
- Sawyer, S.F., Tepper, J.M., and Groves, P.M. (1994a). Cerebellar-responsive neurons in the thalamic ventroanterior-ventrolateral complex of rats: light and electron microscopy. *Neuroscience* 63, 725–745.
- Sawyer, S.F., Young, S.J., Groves, P.M., and Tepper, J.M. (1994b). Cerebellar-responsive neurons in the thalamic ventroanterior-ventrolateral complex of rats: in vivo electrophysiology. *Neuroscience* 63, 711–724.
- Seol, M., and Kuner, T. (2015). Ionotropic glutamate receptor GluA4 and T-type calcium channel Cav 3.1 subunits control key aspects of synaptic transmission at the mouse L5B-POm giant synapse. *Eur. J. Neurosci.* 42, 3033–3044.
- Sherman, S.M. (2014). The function of metabotropic glutamate receptors in thalamus and cortex. *Neuroscientist* 20, 136–149.
- Sherman, S.M., and Guillery, R.W. (1998). On the actions that one nerve cell can have on another: distinguishing “drivers” from “modulators.”. *Proc. Natl. Acad. Sci. USA* 95, 7121–7126.
- Shinoda, Y., Futami, T., and Kano, M. (1985). Synaptic organization of the cerebello-thalamo-cerebral pathway in the cat. II. Input-output organization of single thalamocortical neurons in the ventrolateral thalamus. *Neurosci. Res.* 2, 157–180.
- Smith, A.M., Massion, J., Gahéry, Y., and Roumieu, J. (1978). Unitary activity of ventrolateral nucleus during placing movement and associated postural adjustment. *Brain Res.* 149, 329–346.
- Steriade, M. (1995). Two channels in the cerebellothalamic system. *J. Comp. Neurol.* 354, 57–70.
- Steriade, M., Apostol, V., and Oakson, G. (1971). Control of unitary activities in cerebellothalamic pathway during wakefulness and synchronized sleep. *J. Neurophysiol.* 34, 389–413.
- Stoodley, C.J., D’Mello, A.M., Ellegood, J., Jakkamsetti, V., Liu, P., Nebel, M.B., Gibson, J.M., Kelly, E., Meng, F., Cano, C.A., et al. (2017). Altered

- cerebellar connectivity in autism and cerebellar-mediated rescue of autism-related behaviors in mice. *Nat. Neurosci.* *20*, 1744–1751.
- Teune, T.M., van der Burg, J., van der Moer, J., Voogd, J., and Ruigrok, T.J. (2000). Topography of cerebellar nuclear projections to the brain stem in the rat. *Prog. Brain Res.* *124*, 141–172.
- Tsai, P.T., Hull, C., Chu, Y., Greene-Colozzi, E., Sadowski, A.R., Leech, J.M., Steinberg, J., Crawley, J.N., Regehr, W.G., and Sahin, M. (2012). Autistic-like behaviour and cerebellar dysfunction in Purkinje cell Tsc1 mutant mice. *Nature* *488*, 647–651.
- Uno, M., Yoshida, M., and Hirota, I. (1970). The mode of cerebello-thalamic relay transmission investigated with intracellular recording from cells of the ventrolateral nucleus of cat's thalamus. *Exp. Brain Res.* *10*, 121–139.
- Viaene, A.N., Petrof, I., and Sherman, S.M. (2013). Activation requirements for metabotropic glutamate receptors. *Neurosci. Lett.* *541*, 67–72.
- Wang, S.S., Kloth, A.D., and Badura, A. (2014). The cerebellum, sensitive periods, and autism. *Neuron* *83*, 518–532.
- Yamamoto, T., Noda, T., Samejima, A., and Oka, H. (1985). A morphological investigation of thalamic neurons by intracellular HRP staining in cats. *J. Comp. Neurol.* *236*, 331–347.
- Yoshida, M., Yajima, K., and Uno, M. (1966). Different activation of the 2 types of the pyramidal tract neurones through the cerebello-thalamocortical pathway. *Experientia* *22*, 331–332.
- Zikopoulos, B., and Barbas, H. (2007). Parallel driving and modulatory pathways link the prefrontal cortex and thalamus. *PLoS One* *2*, e848.
- Zikopoulos, B., and Barbas, H. (2012). Pathways for emotions and attention converge on the thalamic reticular nucleus in primates. *J. Neurosci.* *32*, 5338–5350.